Numerical Investigations of Ship Forces During Lockage

Carsten Thorenz[1*] and Lydia Schulze[2*]

Abstract

The evaluation of ship forces for planned or existing navigation lock systems is essential for a sound design in terms of safety, cost and speed. It is a complex task that requires knowledge of physical understanding and modelling of the ongoing hydraulic processes during the lock filling. In this case study, focus is put on the ability to analyse the magnitude of the ship forces with a three-dimensional computational fluid dynamics (CFD) model based on the OpenFOAM® software package. The inhouse state-of-the-art of the ship force evaluation during levelling with the means of three-dimensional numerical modelling is presented. The results are compared to physical model tests at a scale 1:25 and discussed. The outcome shows a very good agreement in terms of flow rates and longitudinal ship forces. The results for the transversal ship forces are promising because the system behaviour is reproduced but the accuracy of the peak values is still to be enhanced. An analysis shows several possible sources for these discrepancies.

Keywords

Navigation lock, OpenFOAM®, CFD, 3D, numerical model, physical model, ship force, filling system

1   Introduction

Navigation lock systems at waterways are designed to enable ships to overcome natural or manmade height differences. Dependent on the height and the desired filling time, different filling systems are used. For lifting heights up to 10 m mostly through-the-head systems are used in Germany, where the water enters the lock chamber from the upstream head. Locks with larger lifting heights are usually more complex with lateral or bottom filling systems to allow a faster filling with larger inflow rates. A comprehensive description of the variety of filling systems can be found in Partenscky (1981), PIANC (1986), Beem et al. (2000) and PIANC (2009). Lock system design is always a compromise between a fast and safe filling and reasonable building and life cycle costs (PIANC 2009 and 2015). Aiming for a fast and safe lockage, the design of a navigation lock system is constrained (amongst other criteria) by the maximum forces acting on the ship. The force restriction is derived from the maximum load that the mooring lines (and the bollards) can bear before failing.It is crucial to limit these forces, as breaking lines can cause danger to life, ships and lock infrastructure. Thus, a smooth levelling process with small forces is a prerequisite for safety and also increases the ease of the levelling

process for the ship's crew. The evaluation of the ship forces for planned or existing lock systems is a complex task that requires knowledge of physical understanding and modelling of the ongoing hydraulic processes during the lock filling. Neither physical scale models nor numerical methods provide all necessary answers easily, because depending on the model type significant modelling efforts, background knowledge about the physics and the bounds of the applicability of the models can be required. With growing complexity of the filling system, the investigation of the ship forces becomes more difficult.

In the literature, the resulting forces during levelling are either described as hawser forces or as ship forces. Ship forces are the direct forces acting on the ship hull which are often measured in physical scale models. Hawser forces describe the forces that are introduced into the hawser lines. These attach the ship to the bollards which are part of the lock structure (PIANC 2009). To account for the dynamic effects in the force transmission process the ship and its mooring lines can be considered as a mass-spring system (De Mulder 2009). Dependent on the pretension of the hawsers, the hydrodynamic force on the ship hull provokes an acceleration of the ship. As a consequence, it starts moving in the direction of the resultant force. With the movement of the ship the mooring lines get stretched and the forces are transferred from the ship over the stretching mooring lines into the fixed bollards. The hawsers have to withstand the quasi-static ship force and the inertial force of the moving ship (Schulze et al. 2017). The actual evolving hawser force depends on variable conditions like e.g. the pretension and the material properties of the hawsers, the length and the sag of the hawsers etc. The modelling of the mass-spring system would bring additional complexity and uncertainty into the modelled system. It is difficult to describe the ship-mooring line system with a simplified model as there are many variable parameters like the line length, pretension (sagging) of the lines, handling of the lines during locking, angle between bollard, line and ship, material and size and degree of wear of the hawsers that are not standardized for the vessel fleet. Furthermore, in physical models the line system is hard to model correctly in a reproduceable way. Thus, in most physical and numerical models for the optimization of lock design, ship forces are considered as the target value instead because they are dependent on less parameters which are not under control of the lock designer. The scientific verification of the regulations for the ship forces is a topic of ongoing research at the Federal Waterways and Engineering Institute. The goal is to find a modernized methodology for relations between ship forces and resulting risks as well as a scientifically based concept for the dimensioning of locks (Schulze and Belzner 2021). Currently, allowable ship forces which are considered to result in acceptable hawser forces are used to evaluate the performance of locks in Germany.

Longitudinal ship forces in well-designed through-the-gate filling systems are mainly caused by the following phenomena (Krey 1914):

- A surge wave triggered by the valve opening and the wave propagation,

- the pressure drawdown due to a filling jet,

- a water level slope due to the deceleration of the fluid.

Additionally, forces from jets which directly hit the hull can be relevant, though this should be avoided. In special situations (e.g. not all valves are operating) with more complex or asymmetric filling conditions or with an asymmetric positioning of the vessel in the lock chamber, relevant transversal forces can occur in addition to the longitudinal forces. In many navigation locks the longitudinal forces are larger than the transversal forces. Thus, the detailed investigation of the transversal forces was often neglected. The book on locks by Partenscky (1981) which serves as a basis for lock design in Germany only gives very little information about the development of transversal forces during levelling. It is assumed that the transversal forces are much smaller than the longitudinal forces. The definition of the maximum ship force limit for a navigation lock is dependent on the country's regulations. Most regulations limit the forces to a fixed threshold dependent on the maximum vessel size (PIANC, 2015). For this case study we do not evaluate the ship forces concerning safety and ease of the locking process but we focus on the ability to analyse the magnitude of the ship forces with a physical scale model and a three-dimensional computational fluid dynamics model.

Physical models are a long-time established tool to evaluate the hydraulic performance of a lock in terms of hydraulic behaviour and resulting ship forces. Already in the early 20th century physical model tests were made to evaluate the performance of the locks of the Kiel Canal (Krey 1914). In the following 100 years this methodology has been used for several lock design projects. More recent investigations are the ones for the new Panama Canal locks (Roumieu et al., 2008), the locks of IJmuiden (Kortlever et al. 2015) and Terneuzen (Nogueira et al. 2019) and the locks of Holtenau and Brunsbüttel (Thorenz 2015).

Apart from a physical model analytical approaches were derived to evaluate the performance of locks. Already in 1914 Krey published equations to estimate the lock filling hydraulics and the ship forces. These were later refined by Schijf (1936), Bleines and Wittmann (1949) and Kolkman (1973). Based on these equations, computer programs were developed to calculate the dynamic behaviour more easily and accurately (de Jong and Vrijer 1980, de Loor et al. 2013). One dimensional numerical models for lock chamber and culvert systems were developed later to evaluate the flow in lock chamber and filling culverts and the resulting ship forces (Schohl 1999). All of these approaches provide significant insight into the lock characteristics but are heavily dependent on calibration parameters. In the past and until today, physical model tests and prototype data were used to calibrate these approaches to a certain lock. Then, the calibrated model could be used for further tests.

In the last two decades, three-dimensional numerical models were more and more used to evaluate the necessary parameters for one dimensional network models. After evaluating the global flow behaviour with 1D-models the calculated flow rates can be used as boundary conditions for local three-dimensional models (Thorenz 2009; Thorenz and Strybny 2012). This approach, belonging to the class of "hybrid modelling" approaches, where models of different kind (e.g. different dimensions or physical and numerical models) are used together, is still state-of-the-art in engineering practise. It was for example used in the design phase of the new Panama Canal locks (Roux et al. 2010, Menéndez et al. 2010, Thorenz 2010) or in the design of the Terneuzen lock (O'Mahoney et al. 2018).

In contrast to the modelling of ships making way, publications for the full three-dimensional numerical modelling of ship behaviour during the lock filling process are rare. Thorenz and Anke (2013) showed numerical modelling of the filling process for the Holtenau locks at the Kiel Canal. This numerical model was compared to physical model results of a scale model (1:47). As the lock has a simple through-the-head filling system, only longitudinal forces were evaluated. The comparison of numerical model and physical model showed a very good agreement of the transient flowrates while filling the lock chamber. For the longitudinal forces the numerical model comprised higher forces than the physical model, though the shape of the transient force curve was similar and followed the physically expected behaviour: The temporal development of the force caused by an initial surge wave followed by a subsequent change of sign of the force into the opposite direction was reproduced. Chevallet et al. (2019) presented three-dimensional modelling results for a through-the-head filling of a lock without a comparison to validation data. They did not compute ship forces in the numerical model, but hawser forces. Though the results for the flow rates seem to be reasonable, the presented forces are spiky and do not resemble the typical, expected development for a through-the head filling system (i.e. the impact of surge waves and jet development) and thus must be doubted.

To the authors of this paper no publication is known, where three-dimensional numerical modelling of the lock filling process was performed and compared in terms of flowrates and both longitudinal and transversal ship forces to physical model results. In this paper the inhouse state-of-the-art of the ship force evaluation during levelling with the means of three-dimensional numerical modelling is presented. Focus is also put on the evaluation of transversal forces that received only little attention in the past. The results are compared to physical model tests at a scale 1:25 and discussed.

2   Testcase

The example lock system represents a lock with three lateral saving basins and a pressure chamber filling system. In the investigated lock system, the total lift height is 18.30 m, the hydraulic length is 200 m and the lock chamber width is 12.5 m. Here, and in the following all values are in prototype scale if not explicitly the opposite is stated. The lock design and size considered in this study resembles currently planned locks at the Main-Danube-Canal in Germany. The filling system was designed as a compromise between filling times, ship forces, building effort and accessibility for maintenance. The lock consists of a lock chamber with a pressure chamber underneath. Both chambers are hydraulically connected with 312 vertical cylindrical filling nozzles inside the floor between both chambers. The three lateral saving basins are connected to the pressure chamber (2.50 m high and 9.50 m wide) via two lateral culverts each of smoothly varying rectangular shape (~7 m² cross section per culvert). Each saving basin has two of these connecting culverts. A vertical lifting valve in each culvert allows the controlled filling operation from the saving basins into the pressure chamber. So, in total six valves control the flow from the three water saving basins.

The placement of the nozzles was derived in an iterative procedure between hydraulical, operational and constructional requirements. Thus, the result is hydraulically "sub-optimal". The 312 nozzles have a diameter of 0.30 m and are arranged

in rows of six nozzles symmetrically across the lock chamber width. The centreline distance between the nozzles is 1.74 m in the row. The centreline distance between adjacent rows is 2.60 m. The rows are grouped in three patches. The following distances specify the distance from the upstream lock chamber wall to the row centrelines: The first patch extends from 24.53 m to 53.13 m, the second from 60.23 m to 146.03 m and the third from 153.13 m to 171.33 m.

For filling the lock chamber, the saving basins are consecutively emptied starting from the lowest basin, followed by the middle basin and ending with the highest basin. When the valves are opened, the water flows freely due to the height differences from the saving basin through the culverts into the pressure chamber and enters the lock chamber from the bottom. The filling from the bottom is supposed to ensure a smooth and fast filling locking process. Each of the basins contains approximately 20 % of the lock chamber volume, therefore 60 % of the filling process is performed with the saving basins. The remaining 40 % of the filling water are drawn from the upstream reach via an additional connection.

In this comparison study, only the first part of the filling process via the lowest of the saving basins is considered because it comprises the most difficult stage of the filling process, i.e. the two upper water saving basins, their valves and culverts are omitted. Figure 1 illustrates the concept of the regarded part of the filling system. The flow originates in the regarded water saving basin (top left), flows downwards into the two nearly horizontal culverts (middle) and then into the pressure chamber (bottom right). There it distributes and then flows upwards through the nozzles into the lock chamber. Attached to each culvert, there are three vertical shafts. The middle shaft contains the valve. The other two shafts serve for mounting the valve bulkheads. Towards the pressure chamber you see additional culvert stubs with one vertical shaft each, one on the left and on the right of each connected culvert. These are the remnants of the cut-off culverts leading to the cut-off water saving basins, which are not regarded in this study.
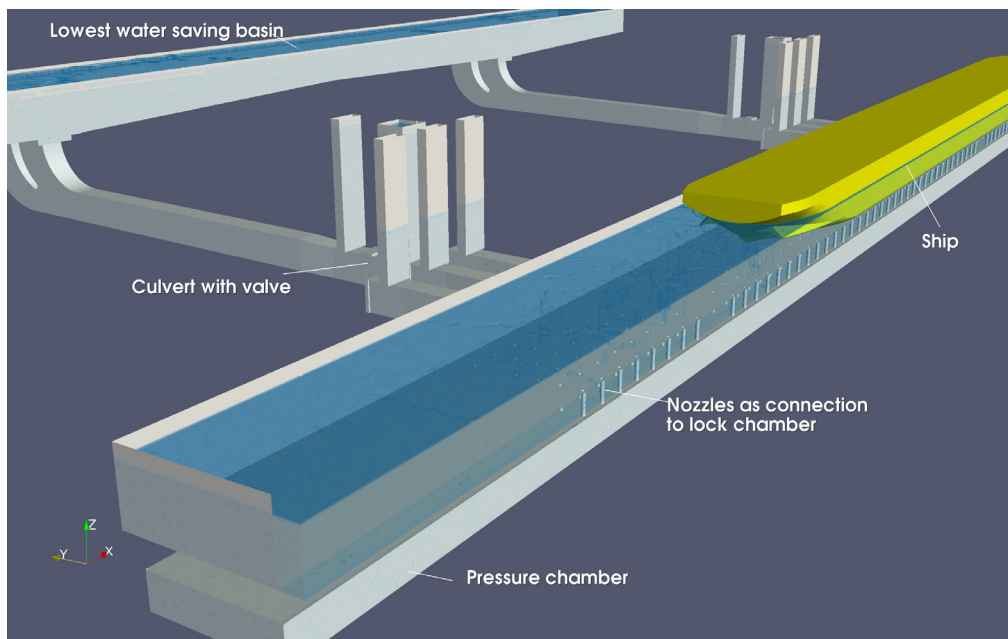

Figure 1: Parts of the hydraulic system as it was modelled in this study. Parts were cut for visualization.

In the described lock longitudinal and transversal forces can occur. An approximate estimation of the forces with simple textbook or 1D-approaches is not feasible, as the flow situation within the lock system is complex. The determination of the exact forces on the ship hull during the lockage is crucial, as the ship forces are the main design criteria for the lock safety. The physical scale model was built to support the design process of the new locks at the Main-Danube-Canal in order to investigate and optimize filling time and ship forces. In the design phase, numerical models were used in a hybrid modelling approach for the optimization of parts of the system as described in the introduction.

To optimize the filling concept for the lock system, the opening and closing speed of the valves were tested in multiple variations with the physical model so that a good compromise between a fast filling and low ship forces was achieved. In this study, we regard only a single valve opening speed, which is in a reasonable range, but not representative for the real lock project.

3 Numerical Modelling

As an alternative to physical scale modelling, numerical models can be chosen to investigate ship forces during lockage. It is a future goal of the BAW to investigate lock filling processes with three-dimensional numerical models. This is part of ongoing research in terms of the usable methodologies in hydraulic engineering. For the lock filling modelling several methods are currently under evaluation. The described lock system was chosen as a testcase in order to evaluate the performance of the modelling approaches for a complex filling system.

To investigate the example lock with pressure chamber and saving basins (as described in section 2), a three-dimensional model of the complete system with a morphing mesh for the ship movement was used. As a numerical code the open source library OpenFOAM® was chosen. OpenFOAM® is a C++ library designed for solving partial differential equation systems. The library provides a large variety of solvers, each designed to model a specific set of physical phenomena. In this case study, the solver *interDyMFoam* from OpenFOAM® version v1812 was used for the simulations.

3.1 Volume of fluid solver

The solver *interDyMFoam* is based on the solver *interFoam* which is widely applied to investigate free-surface flows in hydraulic engineering. *interDyMFoam* shares the same hydrodynamic core but adds the possibility for dynamic mesh manipulation during the computation. *interFoam* is based on the volume of fluid method which was published by Hirt and Nichols in 1980. The solver describes the physics of two immiscible fluids, based on the Navier-Stokes Equations to account for mass (Eqn. 4) and momentum conservation (Eqn. 5) and an additional scalar transport equation to describe the transport of the distribution of air and water (Eqn. 1).

The transport equation for the air-water distribution in the solver is formulated as follows:

$$\frac{\partial \alpha}{\partial t} + \boldsymbol{\nabla} \cdot (\alpha \boldsymbol{U}) + \boldsymbol{\nabla} \cdot [(1 - \alpha)\alpha \boldsymbol{U_c}] = 0 \tag{1}$$

α is the volume fraction of water in each cell in our case study. $\boldsymbol{U}$ represents the transporting velocity of the flow. $\boldsymbol{U_c}$ is an artificial compression velocity. When discretizing and solving the phase fraction equation (Eqn. 1) with the finite volume method, the solution tends to smear the interface between the two phases. To avoid the smearing, the second convection term with $\boldsymbol{U_c}$ is introduced in the *interFoam* solver. The term only acts in the region of the interface between air and water and adds an artificial flux normal to the interface that counteracts the diffusion of the interface. From the solution of α the local density ρ and dynamic viscosity μ can be determined with:

$$\rho = \alpha \rho_1 + \rho_2 (1 - \alpha) \tag{2}$$

$$\mu = \alpha \mu_1 + \mu_2 (1 - \alpha) \tag{3}$$

where ρ_1 is the density of the first phase and ρ_2 is density of the second phase. μ_1 is the dynamic viscosity of phase 1 and μ_2 the dynamic viscosity of phase 2. Mass and momentum equation are formulated for the mixture of both fluids:

$$\boldsymbol{\nabla} \cdot \boldsymbol{U} = 0 \tag{4}$$

$$\frac{\partial \rho \boldsymbol{U}}{\partial t} + \boldsymbol{\nabla} \cdot (\rho \boldsymbol{U} \boldsymbol{U}) = -\boldsymbol{\nabla} p_{rgh} + \boldsymbol{\nabla} \cdot \mu(\boldsymbol{\nabla} \boldsymbol{U} + \boldsymbol{\nabla} \boldsymbol{U}^T) + \rho \boldsymbol{g} + F_{st} \tag{5}$$

where $\boldsymbol{U}$ is the velocity of the mixture, t is the time, p_{rgh} is a modified pressure, where the hydrostatic part of the pressure, consisting of the product of density, gravitational acceleration and the height coordinate is subtracted from the total pressure. F_{st} is the surface tension force that only plays a minor role in the considered case study. With the given formulation of the continuity equation the mixture is assumed to be incompressible with a constant density.

Higher order schemes with total variation diminishing (TVD) properties can be applied for the spatial discretization. Besides that, the OpenFOAM® specific flux-corrected-transport (FCT) algorithm *MULES* (Multidimensional Universal Limiter with Explicit Solution) is applied in a correction step to avoid unboundedness of the results for α. The mass and

momentum equations for the fluid mixture are solved with an iterative pressure-velocity coupling algorithm which is integrated into the fluid structure interaction algorithm. Details of the algorithm are described below (in section 3.3.1).

3.2 Turbulence modelling

Depending on the scales of interest and the computational grid a suitable turbulence modelling concept has to be chosen. In hydraulic engineering the direct numerical simulation (DNS) of the turbulent flow behaviour is rarely feasible for practical purposes due to the necessary extremely fine computational grids. With a substantially coarser spatial discretization, the Large Eddy Simulation (LES) approach can be applied. With this approach, the largest part of the turbulent structures in the flow is directly reproduced and only the unresolved turbulent scales are modelled with a sub-grid scale model (Rodi 2017). Due to the required very fine grid necessary to directly simulate all larger eddies and due to the huge differences in the hydraulically relevant scales (nozzles vs. lock chamber) of the regarded case, a LES model was not used here. Instead, the effect of the turbulence on the momentum transfer is modelled by using the Reynolds-Averaged-Navier-Stokes (RANS) approach together with a two-equation turbulence model. In the following, the k-omega-SST model (Menter et al. 2003) was used. It describes the turbulent kinetic energy and the specific turbulence dissipation rate with the means of two transport equations. After solving these equations, the results are then used to compute the turbulent viscosity field which is added to the physical viscosity of the fluids.

3.3 Fluid Structure Interaction

3.3.1 Bidirectional coupling of fluid and structure

To allow the simulation of the floating ship body within the fluid flow, the fluid solver is coupled within *interDyMFoam* with a six-degrees-of-freedom (6-DoF) body motion solver. The fluid-structure-interaction is modelled with a sequential-iterative method which solves the governing equations of the flow and the rigid body motion with two independent solvers, deforms the mesh accordingly and iterates over the solvers in each time step.

To solve the motion equations for the moving body, the force and moment vectors on the hull of the vessel have to be computed as a surface integral of the normal vectors and the fluid pressure field. Within the discretized numerical model, the resultant force and moment are computed by summing up the shares from all the faces on the ship hull (Eq. 6 and 7). Due to the small impact in comparison to the pressure, shear stresses are neglected here:

$$\boldsymbol{F} = \sum_{i=0}^{faces} \boldsymbol{n}_i \, A_i p_i \tag{6}$$

$$\boldsymbol{M} = \sum_{i=0}^{faces} \boldsymbol{n}_i \, A_i p_i \times (\boldsymbol{x}_i - \boldsymbol{x}_c) \tag{7}$$

with $\boldsymbol{F}$ as the resulting force, i as the index number of the regarded face, $\boldsymbol{n}$ as the surface normal vector, A as the face area, p as the fluid pressure, M as the resulting moment, $\boldsymbol{x}_i$ as the coordinate vector of a face and $\boldsymbol{x}_c$ as the coordinate vector for the centre of rotation of the ship.

It must be emphasized that this procedure is very prone to numerical errors. This is due to the fact that the local forces and moments cancel against each other largely for the ship and are much smaller than the undirected sum of the components. Thus, very small errors in the pressure field can disturb the balance and generate artefacts of a significant magnitude. It must be pointed out that the transversal force is much more difficult to compute than the longitudinal force because the projection area of the side view of the ship is roughly ten times bigger than the projection area of the front view. As a rough estimate for the required accuracy of the force calculation, the transversal forces on each half of the ship can be computed. These are in the order of $\pm 5 \cdot 10^6$ N respectively and should cancel against each other to an acceptable error margin of ~1000 N for this project. Thus, the pressure field at the ship hull must be accurate for four digits.

After computing the force and moment resulting from hydrodynamic effects, the external force components (gravitation, ship positioning equipment) are added. From the results, an acceleration for the linear motion and for the rotational motion are computed from Newton's law of motion. This acceleration is modified with accelerations from

external forces like gravity or hawser forces. The resulting accelerations are then used in a Newmark scheme to compute the new velocity and position within each iteration of a time step. After moving the body to its new position, the mesh has to be adapted to it.

For the mesh motion the displaced boundary at the ship represents a boundary condition and determines the new position of the boundary grid points. To adapt the points of the internal mesh to the new position of the moving object boundary, an additional solver for the mesh deformation is applied. The solver calculates a new position of the internal point motion by solving a motion equation (Jasak and Tuković 2010). In order to maintain the mesh quality, the mesh motion can be characterized with a variety of different equations. For the case study we applied the *displacementLaplacian* solver which describes the mesh deformation with a Laplace equation (Laplacian of diffusivity and cell displacement) (Gonzales 2009). With the Laplace equation for the mesh motion the largest point movement is adjacent to the moving boundary. This can lead to poor mesh quality in the highly deformed cells close to the boundary. An improved behaviour of the mesh motion can be achieved by introducing non-uniform diffusivity (Jasak and Tuković 2010). In the case study example an exponential diffusivity with inverse distance from the rigid boundaries of the nozzles, the side walls of the lock chamber and the ship hull was defined. Therefore, the largest vertical stretching of the cells evolves below the ship in the mid distance between the keel and the lock chamber bottom, whereas the cells close to the listed boundaries mostly conserve their size and shape.

For the rigid body motion the library *sixDoFRigidBodyMotion* is applied which allows to define constraints and restrains for the floating hull. For the case study the ship is fixed with three springs: one spring in longitudinal (x-direction) and two in transversal direction (y-direction). The spring stiffness was adapted to mimic the elasticity of the physical model measuring device, based on measurements of the longitudinal deflection after applying a force in the physical model. The springs had a near infinite length in order to minimize unwanted force components originating from the movement of the spring attachment point at the moving body.

The coupling between the fluid and the solid motion solver is designed in an iterative matter. The number of the so-called PIMPLE iterations defines how often the motion and the flow field are solved within one time step. With this implicit coupling an equilibrium state between the flow field and the motion of the object is aimed at (Devolder et al. 2015). The following flow-chart in Figure 2 depicts the *interDyMFoam* solver algorithm used for the fluid-structure-interaction.
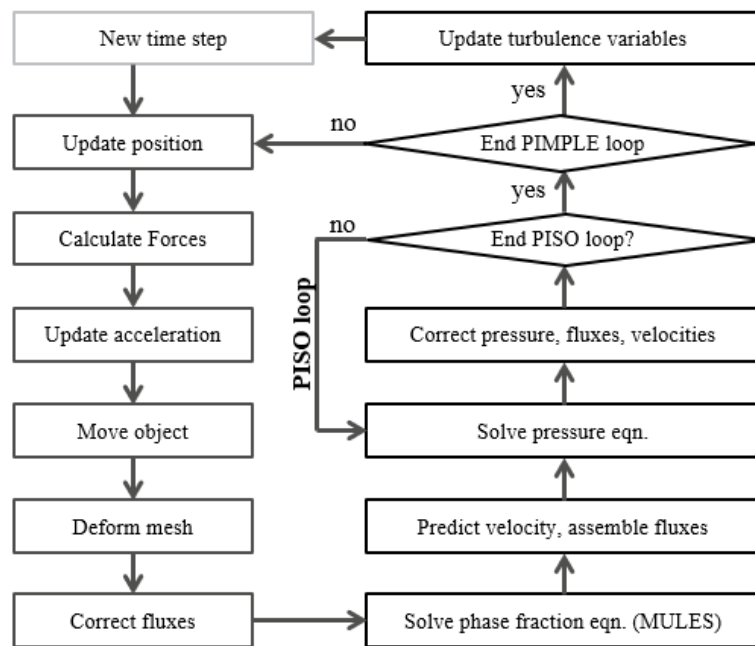

Figure 2: Flow chart of the Fluid-Structure-Solver (adapted from Göbel 2019).

The motion equations can be solved with the Newmark (second order implicit), the Crank Nicholson (second order implicit) or the symplectic scheme (also called leapfrog scheme, second order explicit). In our case study we chose the Newmark scheme to achieve a stable solution.

In the standard solver setting the total acceleration of the rigid body motion can be relaxed with a user-defined under-relaxation factor. Usually, relaxation limits the rate of change in the solution fields which improves the stability of the calculation. However, the case study example showed severe excitement in the mass-spring system through the relaxation of the spring force. To counteract this, the relaxation was turned off for the spring force calculation by changing the source code of the solver accordingly.

3.3.2   Monodirectional coupling at the valves

The valves inside the culverts were modelled as two-dimensional surfaces inside the mesh. With an in-house development, the internal mesh faces which represent the valves are considered either as common internal faces when the valve is open or as impermeable faces when the valve is closed. This was switched dependent on a user-defined valve-opening schedule. The schedule defines the varying opening height of the valve over time. The regarded valve schedule employs an initial 10 s period with closed valves and then a linear opening until the valves are fully opened 40 s after start of the test. The valve stays open until 126 s is reached and then starts to close, ending at 166 s.

3.4   Meshing

For the meshing process a 3D-CAD geometry was generated on the basis of the drawings used to build the physical model. The mesh was created with the OpenFOAM® meshing tools *blockMesh* and *snappyHexMesh*. To find a suitable spatial discretization for the different parts of the lock without getting too many cells for the computation is crucial. In general, zones with large gradients in the flow field variables which are crucial for the system behaviour should be refined in the mesh. In the example lock filling system the mesh had to fulfil several constraints:

-    layer cells near the walls matching to assumed roughness,

-    horizontal grid lines near the water surface in order to avoid initialization errors,

-    high quality cells around and beneath the ship for a good pressure computation and in order to allow subsequent mesh deformation,

-    sufficient resolution in the hydraulically relevant and geometrically difficult parts (e.g. the nozzles, at the valves, at all edges and sudden expansions etc.).

The mesh generation strategy was driven by the experience of the authors from other projects in terms of required grid resolutions for specific parts i.e. near the culvert walls, in the area behind the valves or in areas with large gradients in the flow field on the one hand and the restrictions in terms of available computational resources on the other. In an iterative manner, test computations were performed for meshes with different resolutions in order to check if the necessary mesh motion near the ship could be realized and if the relevant flow patterns could be observed in the simulations. If necessary, the mesh was enhanced and the procedure was restarted. It is important to note that in this iterative cycle geometrical differences between physical model and numerical model were found which could be attributed to discrepancies between the original technical drawings of the project and the realized physical model. The physical model diverted from the desired shape, i.e. due to constraints in the construction. Thus, for this comparison study the CAD model had to be adapted to the realized shape of the physical model. The mesh generation took several iterations of "mesh generation" and "test computation" to achieve sufficient quality.

Figure 3 shows several cross-sections of the final mesh: Note the refinements at the lower tip of the valve position (Figure 3 upper, vertical section of one culvert, flow from left to right, valve marked in red). Especially for small valve openings an emerging jet can be expected behind the valve. Thus, a local refinement with multiple zones was chosen in order to accurately capture the jet behaviour. Furthermore, the mesh directly below the ship (ship marked in dark yellow) was refined anisotropically in order to allow for a sufficient vertical stretching of the cells while moving the ship upwards. Please note, that this layer of cells only allows a limited amount of stretching before the quality decreases too much. We start with a height-width ratio of the cells of 1:2 and think, that a maximum ratio of 2:1 could be acceptable. I.e. the initial

under keel clearance of 1.2 m can be expanded by a factor 4. This limits the acceptable maximum lift height to 3.6 m in this example. Fortunately, the major hydraulic effects occur much earlier in the filling process. For higher lifts, topological changes to the mesh would be required.
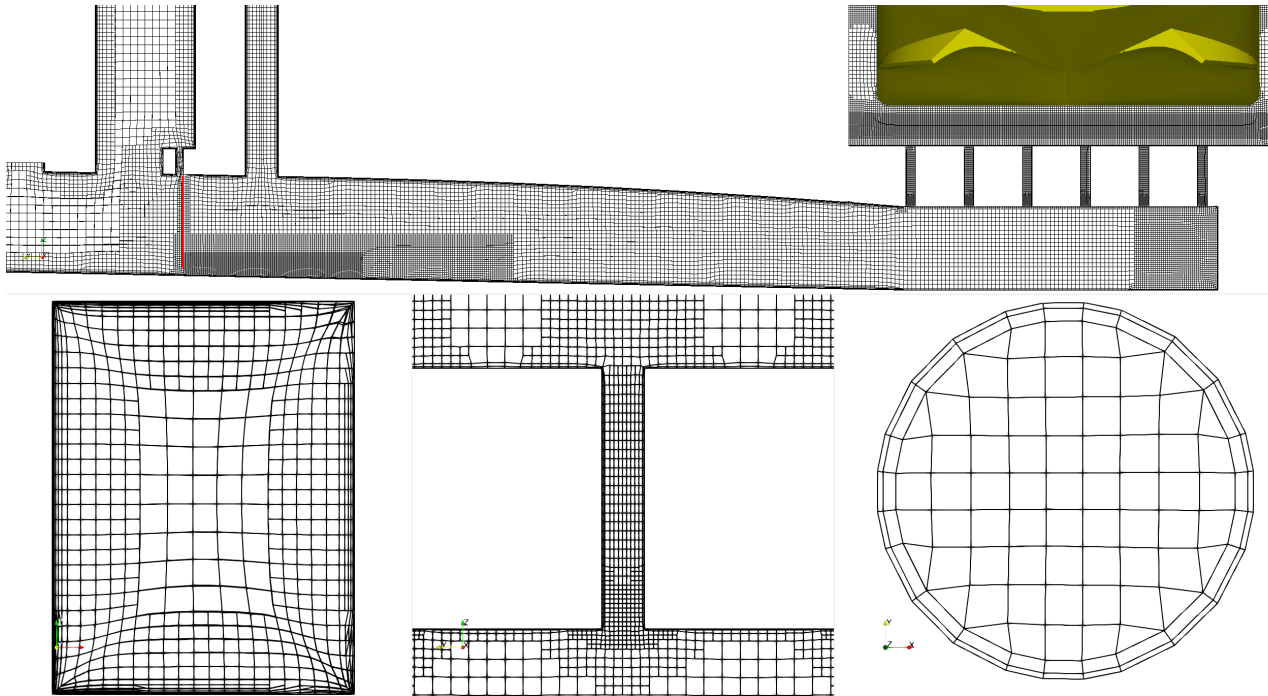

Figure 3: Upper: Vertical section of the mesh along one of the culverts with the position of the valve denoted in red and the ship in yellow plus a section through a nozzle row. Lower (left): Cross section of a culvert. Lower (middle): Vertical section through a nozzle. Lower (right): Horizontal section through a nozzle.

For a proper computation of the head losses due to friction in the culverts (varying cross-section of approximately 8 m²) a fine resolution at the culvert walls with a smooth mesh gradient towards the walls is desirable. The thickness of the cells at the wall should be small enough to accurately reproduce the momentum transfer to the wall and on the other hand must not be too small, because this would result in failure of the wall boundary conditions to replicate a desired roughness. Thus, a mesh with layer cells of ~0.006 m thickness at the culvert walls and an expansion ratio of 1.5 away from the wall was generated (Figure 3, lower left). This was assumed to be suitable for the expected roughness. The finest cells were used at the entrance areas of the nozzles because a flow separation was expected at the edges (Figure 3, lower middle and right). In the nozzle entrances a base edge length of ~0.03 m was chosen with a further wall parallel refinement to ~0.01 m. The upper part of the nozzle was refined anisotropically. As there are 312 nozzles with 0.30 m diameter in the system and each nozzle is 1.80 m long, this resulted in a substantial number of cells and was regarded as the highest feasible resolution. Based on these requirements, finally a hexahedra-dominant body fitted mesh with 27 907 672 cells was generated. Figure 4 presents an overview of the cell sizes in the generated grid on the basis of their cell volume. It must be noted that some cells are not cubic (i.e. near the walls, in the expected jets and under the ship) and thus the cubic root of the cell volume can only be used as a hint for the cell size.
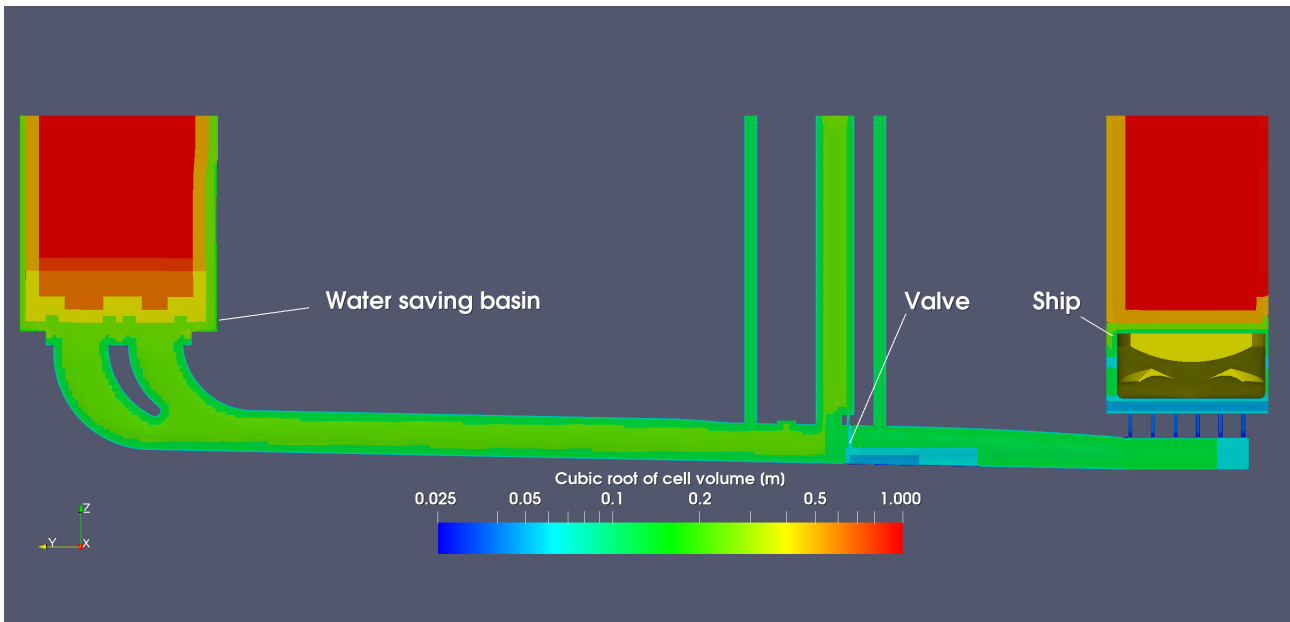
Figure 4: Vertical cross-section of the mesh in one of the culverts showing the computational cell size.

In many numerical projects it is good practice to perform a grid convergence study in order to verify that the mesh resolution is sufficient for the given problem. This is necessary but not a sufficient condition in order to show that a numerical model is able to have predictive capabilities for a given questions.

Here, the situation differs. This study did not aim at generating predictions from the numerical model for a real project but is aimed at showing the modelling procedure with its necessities. It can be regarded to be on the edge of what is feasible in high-level engineering today. The requirements for the meshing mentioned above resulted in a grid which consumes substantial computational resources for the simulations. It did not allow for a formal grid convergence study, as a further refinement of the whole system would have resulted in a mesh with over 200 million cells and would have increased the computation time at least by a factor of 16 due to the required halving of the time step size. Thus, a computation for a further refined mesh would not have been feasible anymore. For parts of the mesh the refinements were chosen due to prior experiences and for other parts, separate computations were performed in order to check the plausibility of the observed flow pattern. This requires a high level of experience in both hydraulics and numerical methods. Anyhow, later analysis showed that some parts of the mesh had a critically low resolution. This is presented in Section 4.3.1.

3.5 Initial and boundary conditions

An essential prerequisite for the simulation of a lock filling is the initialization process. Here, the lock chamber was filled up to a level of 4 m with water. The culverts and saving basins were filled to a level of 11.27 m relative to the lock chamber floor. After successful initialization, the velocities of fluid and ship should be close to zero and the vessel should be floating freely with no relevant forces required to keep it in place. From the experience of the authors the initialization process is a challenging task when simulating a lock filling process. The centre of gravity and the mass of the ship must be calibrated very carefully to avoid initial disturbances when starting the simulation. It is a requirement for the quality of the following simulation to prove the satisfactory adjustment of the initial conditions. This is achieved by simulating a no-flow situation with a floating vessel. The resulting forces on the vessel must be below the required error margins for at least the time of the natural period of the sloshing water in the lock chamber. Here, we achieved to stay below a remaining ship force of 1 kN resulting from the initialization disturbance.

For the fluid and the rigid body motion solvers boundary conditions (BCs) have to be defined for each boundary patch. In the case study, the boundaries can be divided into four categories:

- fixed walls with stationary mesh,

- fixed walls with sliding mesh,

- moving patches and

- atmospheric boundaries.

In terms of the dynamic mesh, the fixed walls define the boundaries that remain unchanged during the complete moving mesh procedure. The ship hull has to be defined as a moving patch where the velocity of the boundary is determined with the 6-DoF body motion solver. It is defined as *sixDoFRigidBodyDisplacement*. As the body is assumed to be solid and not deformable, the mesh points on the boundary are not moved relatively to each other, but the complete boundary patch is allowed to move inside the mesh based on the equations of motion for the ship. In the example navigation lock system, the lock chamber side walls and the back and front wall of the lock chamber are defined as fixed walls with sliding mesh. The mesh points are allowed to move along these boundaries on a plane with the *fixedNormalSlip* condition. With that, the mesh deformation due to the moving boundary of the ship can be minimized near the walls.

From a fluid mechanics point of view, we can distinguish closed boundaries and open boundaries in the model. For the closed boundaries (all walls and the ship) a zero-gradient BC for the non-hydrostatic pressure and a fixed velocity was set. The fixed velocity was set according to the movement speed of the boundary, i.e. equal to zero for all walls and equal to the actual movement velocity field for the ship. The moving wall velocity condition corrects the flux due to mesh motion such that the total flux through the moving wall is zero. For the turbulence model the turbulent kinetic energy was defined by the *kqRWallFunction* and the specific dissipation rate was defined by the *omegaWallFunction*. The turbulent viscosity was computed by OpenFOAM®'s *nutkRoughWallFunction*. This approach is not the obvious choice to compute the friction impact of smooth walls but it was a necessary workaround in order to allow an adaption to the physical model friction impact. For the open boundaries at the top of the model, the pressure is fixed to atmospheric pressure. The velocity is calculated as zero-gradient and thus the air can exchange freely with the model.

3.6 Solver settings and discretization schemes

The time-integration for the fluid solver was solved with an implicit scheme. The time stepping size was dynamically adapted on the basis of the Courant-Friedrichs-Levy (CFL) number. For the simulations a maximum CFL number of four was allowed. For high CFL numbers a lower quality of the results must be expected. But typically, during the simulations the maximum CFL value was only reached in a very few cells of the model. The distribution of CFL numbers varied during the course of the simulation. Typically, 95 % of the cells showed CFL numbers below 0.5 and more than 99% showed CFL numbers below 1.0. Thus, most cells do not suffer from an accuracy reduction due to the time step size. The resulting time steps had a range from 0.003 s to 0.040 s for a highly optimized mesh adding up to approximately 40 000 time steps per simulation.

For the advection terms of the momentum equations and the transported quantities (turbulence quantities, volume of fluid function) second order accurate discretization schemes were selected for CFL numbers below 0.5. These are linearly blended to upwind schemes for CFL ≥ 2. As a result, for ~95 % of the cells a second order accurate scheme was used. For a further 4 % of the cells a scheme was used that had at least a 66 % weighting towards second order accuracy.

3.7 Parallel computing

Large simulation cases, as this lock filling example case, are nowadays computed in parallel. For that, the mesh and the associated fields are decomposed and allocated to separate processor cores for the calculation. This domain decomposition is based on the Message-Passing-Interface (MPI) and is widely used in computational sciences. OpenFOAM® was built taking MPI into account and thus largely gains performance from the decomposition. The decomposition process aims at a decomposition with a small number of processor boundaries. The example case was decomposed with the *Scotch* decomposition method (Pellegrini 2009). The computations were performed on two different cluster computer systems. On the first machine the best parallel efficiency was observed for 240 CPU cores (~105 000 cells/core). A very good parallel scaling was observed up to 800 CPU cores (~32 000 cells/core). For this

number of cores still 90 % of the optimal computing efficiency was reached. On the second machine the optimal performance was observed for 768 CPU cores (~33 000 cells/core) with an efficiency above 90 % for up to 1 280 cores (~20 000 cells/core). For this study, so many CPU cores were not always available and differing core numbers were used for the simulations presented here. The computing time for one of the runs was ~268 000 s (more than three days) on 896 cores (i.e. $2.4 \cdot 10^8$ CPU core seconds) for a simulated time of 200 s.

3.8 Calibration

Flows in the near-field of hydraulic structures are typically dominated by the geometry of the structure. Therefore, calibration should not be necessary for a three-dimensional numerical flow model of sufficient numerical quality because friction is a minor factor. If calibration is performed, this should have a sound physical background and stay within reasonable and expected physical margins. Here, different materials were used in the physical model to build the filling system and these are partially smooth and partially machined. Thus, the friction properties of the filling system are not exactly known but it was estimated that the equivalent sand grain roughness must be in the order of tenth of millimetres or below in the physical model (model scale).

With the wall-functions commonly used for rough walls (e.g. for concrete surfaces) it was doubted if the pressure drop within the acrylic glass culverts of the physical model could be reproduced with the generated mesh. In order to check that, a simplified model of only a single culvert was set up and the computed pressure drop per meter length due to friction was compared to values from the Colebrook-White / Darcy-Weisbach formulae. It was tested, if this numerical model could reproduce the expected pressure drop for roughness heights of 1 mm to 5 mm (prototype scale) for a prescribed stationary flow. As this was in good accordance, the mesh was accepted. It was decided to test different roughness values for their accordance with the physical model results. In the following, equivalent sand grain roughness height variants of 1 mm, 2 mm and 5 mm, set for all walls, were tested. This is equivalent to 0.04 mm, 0.08 mm and 0.2 mm roughness height in physical model scale.

3.9 Fluid properties

As the physical model was originally built to enhance the design process for a real-world project, all results of the physical model were immediately recalculated to prototype scale by the logging software. In order to facilitate comparison, the numerical model was thus also setup in prototype scale. As the physical model is set-up on the basis of Froude similitude, it is well known that the turbulent regime cannot be exactly the same as in the prototype scale due to the differing Reynolds numbers. As the numerical model was built in prototype scale, it was decided to adjust the dynamic viscosity in the numerical model for the sake of Reynolds similitude with the physical model. Thus, the dynamic viscosity in the numerical model was increased by a factor of 125 in order to match the turbulent behaviour of the physical model. By this means it was possible to do the computations in prototype scale but with the same Reynolds numbers in physical and numerical model.

3.10 Description of the physical model

In the hydraulic laboratory of the Federal Waterways Engineering and Research Institute a model of the above described lock system was built at a scale of 1:25 (Figure 5). The lock chamber, the pressure chamber and the lateral connection channels to the saving basins were constructed from acrylic glass to enable visual investigation of the flow. The upstream and downstream harbour as well as the saving basins consist of plastered brickwork. The whole setup including necessary lab facilities extends over an area of approximately 250 m², with a dimension of the lock chamber of 8.2 m x 0.5 m. The model was built on the basis of Froude similarity. In the following, all values are converted into prototype scale if not the opposite is stated. For this transfer, the scaling laws resulting from Froude similitude were used.

For the filling operation, six engine driven valves were installed inside the channels. To allow the investigation of a large variety of filling scenarios, each valve can be operated separately and can be adapted to different speeds. Within the lock chamber a large self-propelled barge with a prototype length of 134.88 m, a width of 11.43 m and a draught of 2.80 m was installed. The size of the model ship corresponds to the largest authorized ship in the lock and is therefore used to

optimize the lock design. The vessel was placed asymmetrically in the lock chamber: The distance to the lock chamber walls was 3.12 m between bow and upstream wall, 63.00 m between stern and downstream wall, 0.25 m between starboard side and wall and finally 0.82 m between portside and wall. At the bow and at the stern two force sensors record the longitudinal and transversal forces acting on the ship hull. At the bow, longitudinal and transversal forces are recorded, whereas at the stern only transversal forces are gathered by the sensor (force/torque sensor at the bow: Schunk FTN-Nano-17 SI-12-0.12; range of measurement recalculated to prototype scale ±187 500 N, measuring accuracy <1 875 N; force/torque sensor at the stern: Schunk FTN-Nano-17-T SI-8-0.05; range of measurement recalculated to prototype scale ±125 000 N; measuring accuracy <1 250 N). The sensors on the ship are connected to vertical bars which can slide upwards in an elevator. This fixes the position of the ship in longitudinal and transversal direction and fixes the rotation around the vertical axis. Pitch, roll and vertical movement of the ship are unhindered. To minimize movements of the ship in the other directions during the filling process, the bars attached to the elevator rails were constructed from carbon fibre reinforced polymer (a material with a relative high stiffness). The natural frequency of the mass-spring system "ship – elastic measuring device" was significantly higher than the natural frequency of the sloshing water in the lock chamber in longitudinal direction.
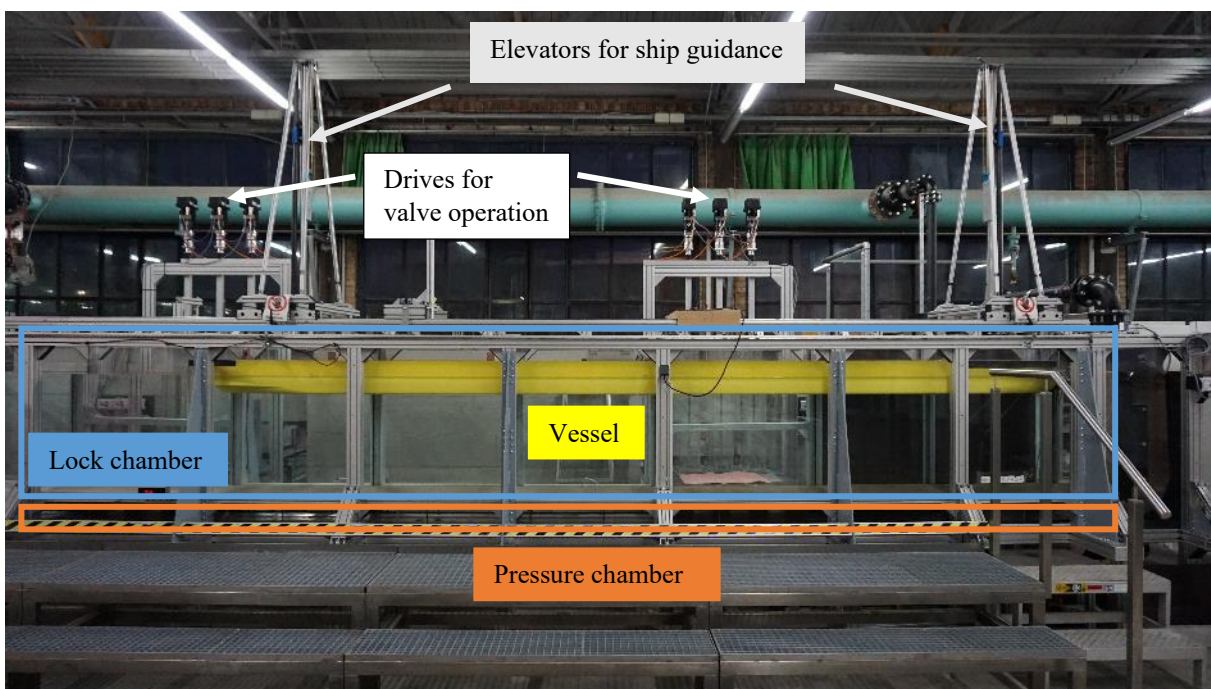

Figure 5: Physical model of the lock with 135 m long vessel (prototype length).

For measuring the water levels in the lock chamber two float gauges are installed at both ends of the lock chamber. For the saving basins lateral measuring pots are used, which are hydraulically connected to the saving basins. In these, ultrasonic sensors perform the actual measurement. To additionally capture water level differences along the longitudinal axis of the lock chamber five differential pressure sensors are installed along the lock chamber wall (water saving basin side) near the bottom. They measure water level differences between two adjacent points within the lock chamber. The first measuring position of the first sensor is located 0.05 m (model scale) from the upstream chamber wall, all further differential pressure sensor measuring positions follow along the longitudinal axis with an equal spacing of 1.59 m (model scale). All water level and force sensor values are directly accessible via the operating program which also allows the operation of the valves. With prescribed valve opening schedules, the defined experiments are executed. For the case study discussed here, the valves stay closed for an initial period of 10 s. After that they start to open with a constant velocity, until they are fully open at 40 s after the start of the experiment (30 s opening time). The valves close in the period 126 s to 166 s. Due the similitude laws this translates to a valve opening starting after 2 s in the physical model, a time of 6 s for opening and after further 17 s the valves start to close again. The water levels and forces data are automatically recorded amongst other data during the lock filling experiments and are instantaneously recalculated to prototype scale.

3.11 Comparison of physical and numerical model results

3.11.1 Introduction

The results of the numerical model tests are presented in the following and validated against physical model results. In the numerical model, a much larger amount of data is produced than in the physical model. Velocities, pressures etc. can readily be measured at any point of the domain. This is practically impossible in physical models. Thus, it is necessary to choose data sets for comparison which are available in both models, which are crucial for the system behaviour and which are easy to compare.

For a quantitative analysis of the results three quantities were evaluated and compared to the physical model results:

- The discharge into the lock chamber,

- the longitudinal forces on the ship hull and

- the transversal forces on the ship hull.

The discharge is significantly influenced by the valve opening speed and the flow resistance of the complete filling system. Thus, the evaluation of the discharge can show how good the valve opening and the discretisation of the complete filling system meets the physical model results. The longitudinal and transversal forces play a major role for the evaluation of the lock design. Therefore, the analysis of the forces is most relevant to judge the applicability of the numerical model for the design evaluation.

3.11.2 Comparison of flowrates

The most obvious entity for comparison in a lock filling process would be the development of the water levels. But due to the integrative nature of the filling process differences are hard to spot. Thus, we chose to compute the flowrates which give a much sharper insight. In the physical model, the flowrates were not directly measured. Instead, they are computed from the development of the water levels in the lock chamber. This proved to be difficult, as waves establish in the lock chamber and noise in the data amplifies in the necessary differentiation. In order to take care of the waves, we used the combination of the float gauges and differential pressure sensors to set up two chains of water level measuring points, starting from each of the two floating gauges. Afterwards, the results of the two chains were used to compute a spatial mean water level. In order to minimize the noise, the water level data was smoothed with a 5 s moving averaging filter for the flowrate computation. Later evaluation of the data showed a small time shift in the data. This was attributed to the mechanical properties of the valves which are mechanically pretensioned in the closed position and thus do not start to open immediately when the drives start. Consequently, all physical model data presented in the following was shifted by -3 s in order to compensate for this effect. In the numerical model the flowrates can directly be measured by integrating the flux over cross-sections of the culverts.

In the quantitative analysis four results are compared: the physical model test and simulations with three different equivalent sand grain roughness heights (as described in section 3.8). The "equivalent sand grain roughness height" is shortened to "roughness" in the following.

In the following we compare three aspects of the hydrograph:

- The incline during the first phase of the valve opening.

- The peak flowrate.

- The decline with fully opened valve after inertia has levelled out.

The comparison of the hydrograph computed from the physical model data and from the different parameterizations of the numerical model is presented in Figure 6.
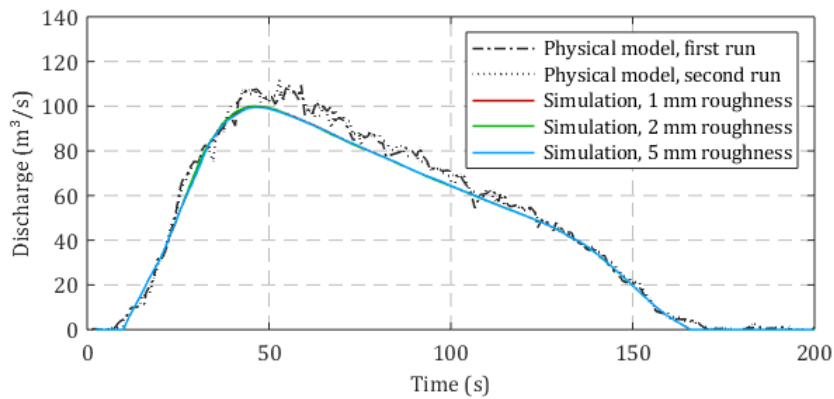
Figure 6: Comparison of flowrates computed from physical model results with numerical simulation results.

The initial incline of the flow rate (Figure 6, 10 s < t < 25 s) is governed by the linear increase of the valve gap. All regarded variants of the numerical model fit very well to the physical model results. This indicates a good representation at the valve.

Comparing the peak flow rates (Figure 6, 45 s < t < 55 s) shows that all simulations underestimate the discharge peak slightly. The roughness variation has only little impact on the peak flow rate.

The slope of the decline of the discharge (Figure 6, 70 s < t < 120 s) reveals whether the total hydraulic resistance of the system is accurately reproduced. The slightly smaller slope of the simulations indicates a too high resistance which is nearly independent from the friction induced by the roughness.

In general, the accordance of the flowrates computed from the physical model results with the flowrates directly measured in the numerical simulations is satisfying.

3.11.3 Comparison of forces

As discussed before, the correct computation of the resulting ship forces of the moving ship is substantially more difficult in a numerical model than computing the mere hydraulic properties. In the following we compare the longitudinal and the transversal force separately.

Comparing the longitudinal force progression over time with the valve motion it is apparent that the opening of the valve provokes a force in longitudinal direction pushing the ship hull towards the upstream end of the lock chamber (positive values in Figure 7). The rise of the longitudinal force starts at the valve opening (10 s) and reaches its highest value at ~30 s. Then, the longitudinal wave in the lock chamber is reflected and results in a reversal of the longitudinal force towards the downstream end of the chamber. The second, negative peak of the longitudinal force after this is much smaller than the first. These forces originate from the asymmetric placement of the ship in the chamber.
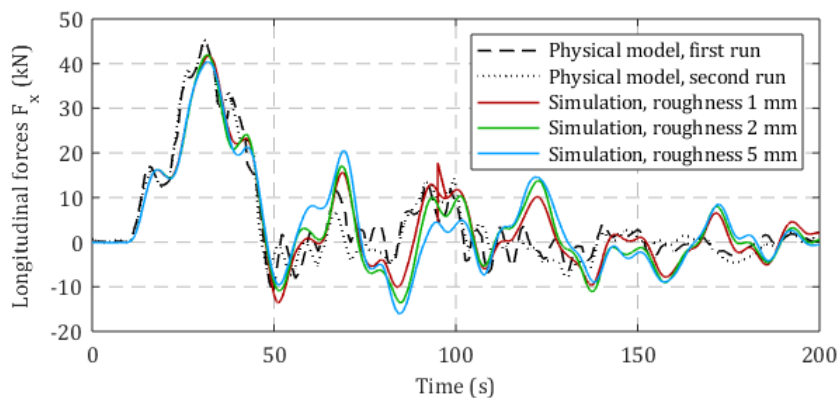

Figure 7: Comparison of longitudinal forces from physical model results with the numerical simulation results.

The longitudinal forces measured in the physical model generally show a very high agreement in size and direction with the numerical model simulations for the first 50 s, where the first and most relevant longitudinal force peak occurs. It is interesting to note that all numerical variants meet the force peak size with only very small impact of the roughness. All variants stay within a 10 % deviation in comparison to the physical model. The time of the occurrence of the maximum longitudinal force only shows minor deviation. In the further course of the filling process, the longitudinal forces show oscillations which are much smaller than the first peak. These are caused by the wave systems in the lock chamber interacting with the ship. These differ more significantly between physical and numerical model, but this is explicable as the mechanical properties of the ship guidance in the physical model are not completely known and are replicated by simple springs in the numerical model. It must be noted that these later results are less relevant for the lock design, as the design is governed by the peak forces.

In general, the accordance of physical and numerical model results is excellent for the longitudinal forces. It must be pointed out that repetitions of physical runs typically also deviate from each other in a comparable manner.
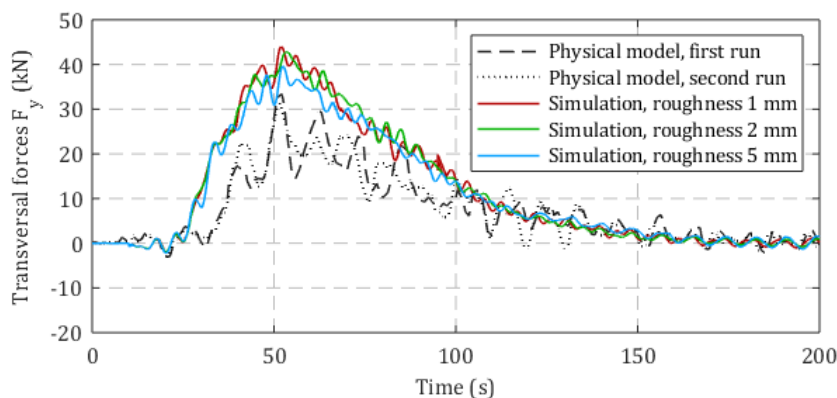

Figure 8: Comparison of transversal forces from physical model results with the numerical simulation results.

In the graph with the transversal forces on the ship hull (Figure 8) positive values indicate forces which push the ship away from the wall into the direction of the saving basins. For the transversal forces, the numerical results differ more significantly from the physical model measurement. Whereas the first peak of the transversal forces in the numerical simulations appears to be at the same time as in the physical model, the magnitude of the maximum transversal forces shows larger deviations.

It is obvious that the numerical model overestimates the peak value. Though not perfect, the accordance is still satisfying as the general system behaviour is captured. The shape of the force curves is comparable. As stated in section 3.3.1, the modelling of transversal forces is much more difficult than modelling the longitudinal forces because the projected area of the ship is much bigger and thus much smaller pressure differences are relevant. Thus, the results are promising but obviously further improvements would be desirable.

4   Further analysis of the results

4.1   Analysis of recorded ship forces

The recorded longitudinal forces are equivalent in the physical and the different numerical models from an engineering point of view (Figure 7). Here it is interesting to note that the peak value occurs at ~30 s. This is before the valve is fully opened (40 s) and before the maximum flow rate is reached (~50 s). It can be deduced that the longitudinal forces are not governed by jet effects in the lock chamber because those effects would occur with or shortly after the highest flow rates. Instead, we conclude that the maximum force corresponds to the rate of increase of the flow rate. Further tests for the engineering project (not presented here) have shown that a slower opening of the valve decreases the maximum of the longitudinal forces much more than it decreases the maximum of the flow rate.

For the transversal forces, the different models provide differing results (Figure 8). Anyhow, the results show that in both the physical and the numerical models the peak force occurs after ~50 s. This corresponds to the time when the maximum flow rate occurs. This leads to the assumption that the transversal forces are triggered by jet effects which are related to the flow rate. Further tests for the engineering project (not presented here) have shown that a slower opening of the valve decreases the maximum of the transversal forces more than it decreases the maximum of longitudinal forces.

4.2 Analysis of flow features

All of the following analysis refers to the variant with 2 mm equivalent sand grain roughness height. The visualization of the velocity field inside the culverts and the pressure chamber (Figure 9, at 30 s simulated time) shows the complexity of the flow field. We can see the jet behind the partially opened valve in the culvert oscillating up and down and also the turbulent regime, where the jet hits the opposite wall of the pressure chamber. It is interesting to note that the flow through all the nozzles has already started, even though the water from the valve has not yet "reached" the nozzles. This is due to the fact that the pressure wave travels much faster than the water itself and thus the increased pressure of the still water triggers the flow to run through the nozzles.
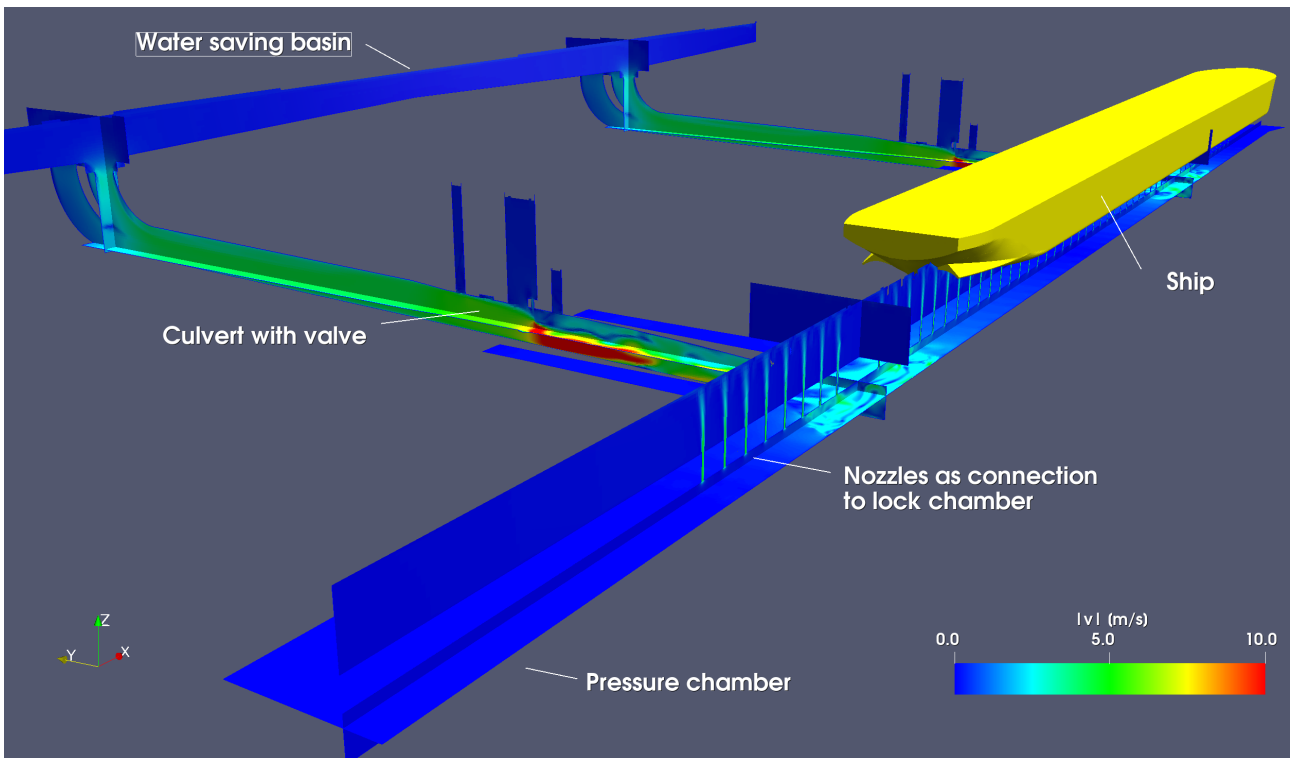

Figure 9: Visualisation of the velocity field after 30 s in multiple planar sections, limited to cells containing water.

A more detailed view is presented in Figure 10. We look at the area where the upstream culvert is connected to the pressure chamber in horizontal slices through the pressure chamber and part of the culvert. The upper subfigure shows a slice 0.2 m below the ceiling, the middle one is located in the middle of the pressure chamber and the lower subfigure shows a slice 0.2 m above the floor of the pressure chamber. It is obvious that the jet from the culvert reaches the opposite wall only in the middle section. In the other planar sections, we can see upwelling and downwelling flows which are the result of swirling corner vortices.
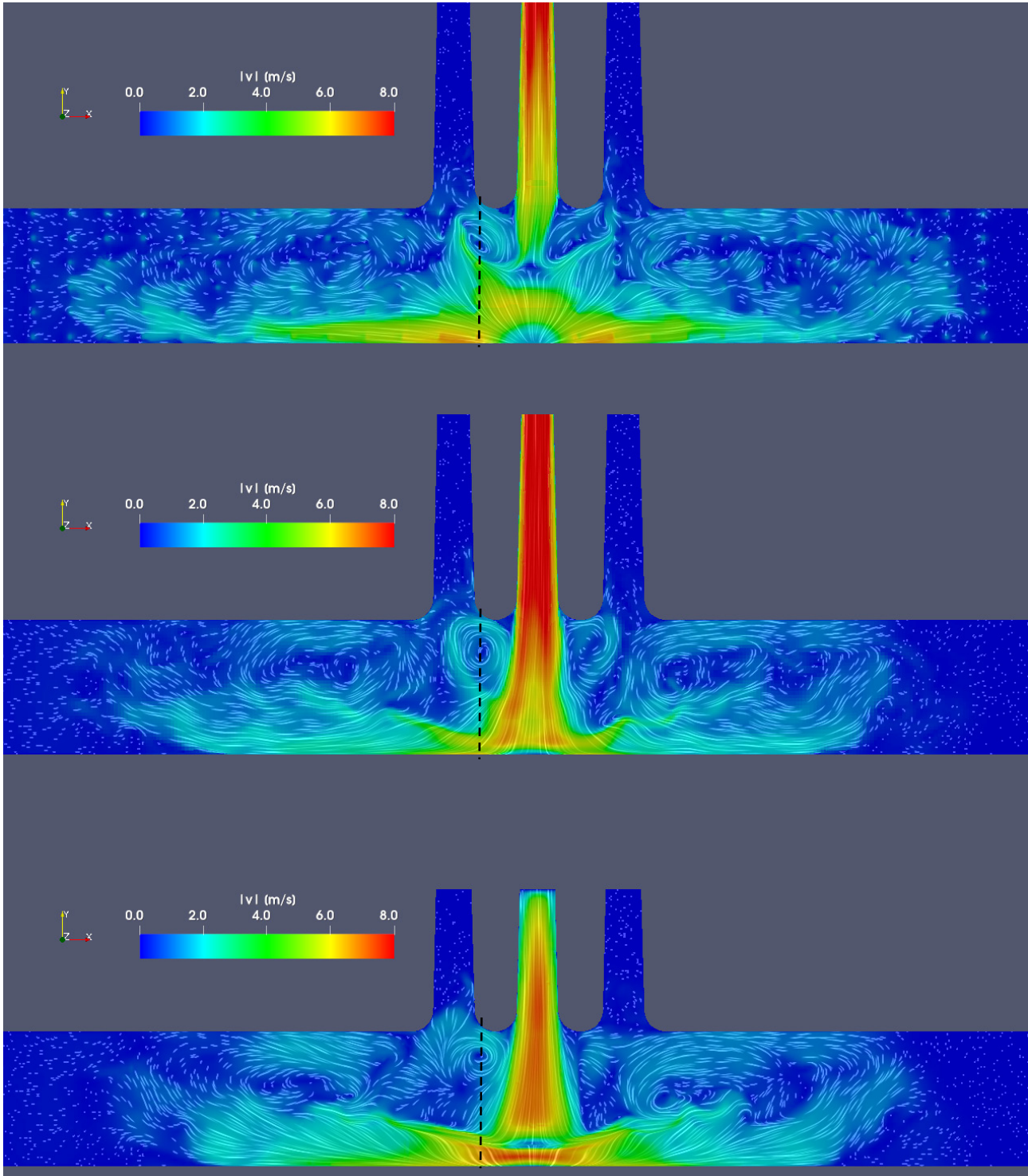
Figure 10: Velocity field after 50 s in horizontal cross-sections through the pressure chamber. Upper: 0.2 m below the ceiling. Middle: in the middle of the pressure chamber. Lower: 0.2 m above the sill. Colour tint indicates the velocity magnitude, texture streaks indicate the flow direction. The dashed line indicates the position of the section in Figure 11.

A vertical cross-section is presented in Figure 11. It shows the ship on top (yellow) and the flow velocities in the lock chamber, some nozzles and the pressure chamber below it. Please note that the ship is placed slightly asymmetrically in the lock chamber, visible from the distances between the ship and the chamber walls left and right. The slice is located at the dashed line indicated in Figure 10. As the slice cuts through the trumpet shape outlet of the culvert, the pressure chamber seems to be asymmetric to the nozzles. This is not the case in most of the system. In the lower right corner, we see a small corner vortex with high velocities. This explains the structure of the flow field near the wall as seen in

Figure 10 (lower). As these corner vortices expand from the impact point of the main jet to both sides, they expand into two corkscrew vortices.

Furthermore, we see a large jet like flow near the ceiling flowing back in the direction of the water saving basins (to the left). This is the source of the "upwelling" seen near the wall in Figure 10 (upper). A closer look at the nozzles (Figure 11) shows flow separation zones in the nozzle inlets due to the high horizontal velocities at the pressure chamber ceiling. The jets emerging from the nozzles rise upwards towards the ship and cause smaller and rather slow eddies between the jets.
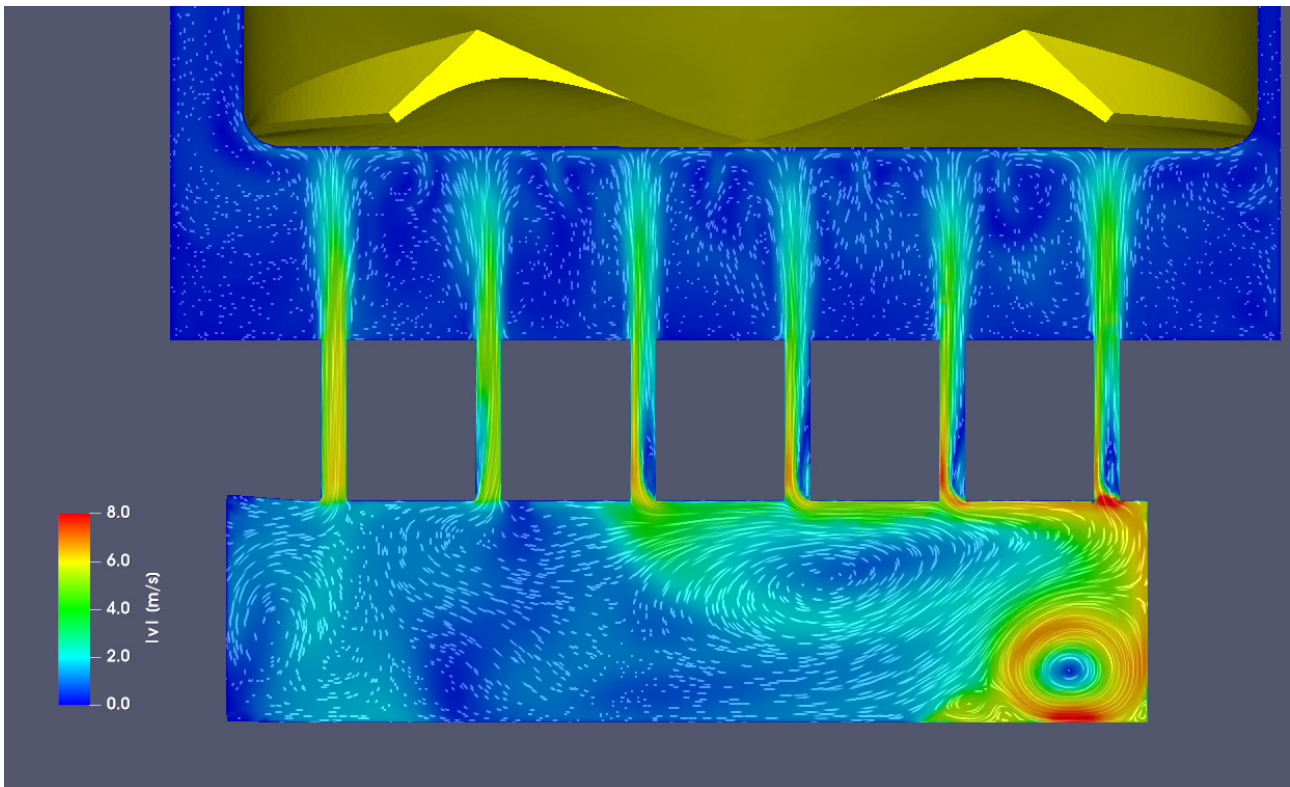

Figure 11: Velocity field after 50 s in a vertical cross-section as shown as dashed line in Figure 10. Colour tint indicates the velocity magnitude, texture streaks indicate the flow direction. The water saving basins are located at the left.

Summarizing, the flow field in the pressure chamber is constituted from a complex system of jets and eddies which seems to be rather delicate. It is difficult to perform a detailed comparison between numerical and physical model results for this situation, as the area is not accessible in the physical model.

From an engineering point of view, it is relevant to enhance the price/benefit ratio of the construction. For a good navigation lock it is a goal to enhance the speed of the filling without compromising the safety or the cost. In order to check the hydraulic performance, it can be helpful to examine the energy losses in the system. Due to the dynamic effects, this can only be done at a time when the change of the flowrate is negligible. Thus, we have chosen the time t=45 s for examination, because the change of the flowrate is minimal at that time. The numerical model results offer the possibility to analyse the flow at any point of the model. Figure 12 shows the computed energy height in multiple cross-sections of the model. Following the flow direction, we see a small energy loss from the water saving basin to the culvert (~ 1 m energy height difference), a significant energy loss from the culvert to the pressure chamber (~3 m energy height difference) and a further significant loss at the nozzles (~ 2.5 m). From a hydraulic designer's point of view, the system should be governed by the energy losses at the nozzles, as these serve as a throttle to enhance the distribution along the lock length. On the other hand, the loss between culvert and pressure chamber is unwanted and thus leaves room for further optimization.
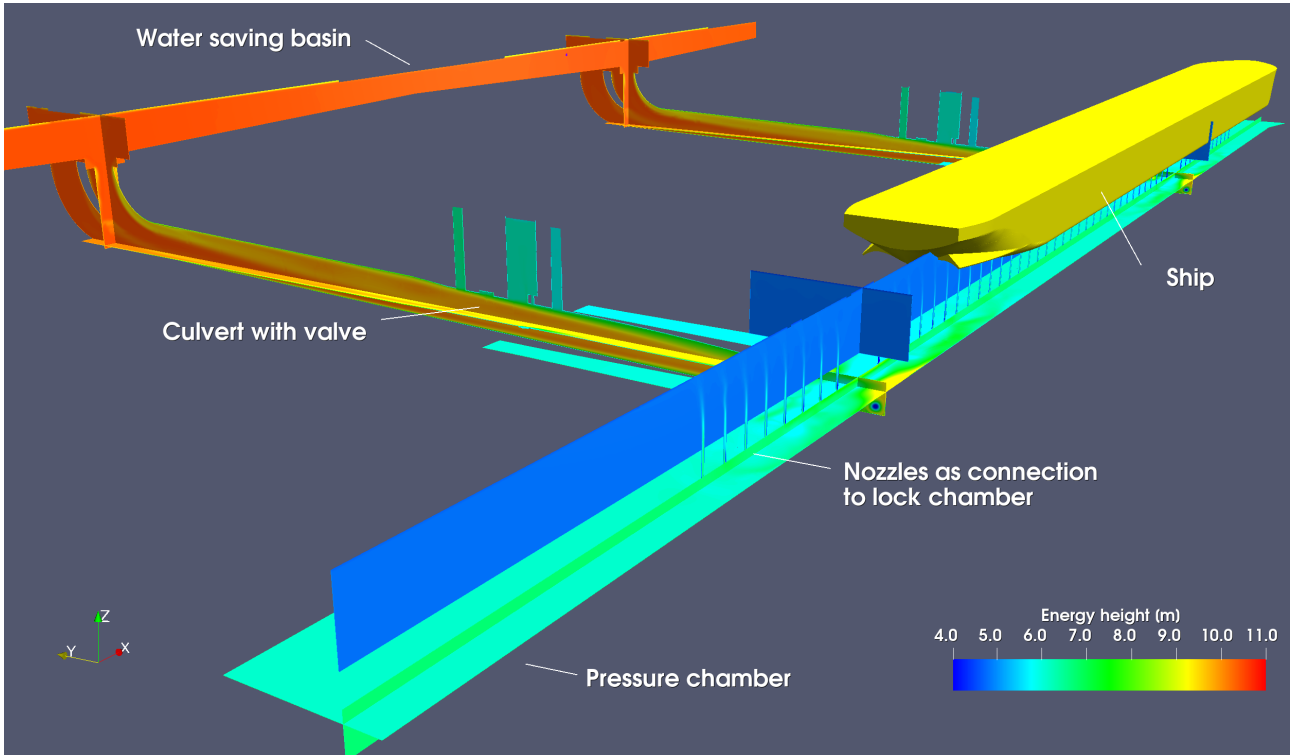
Figure 12: Visualisation of the energy height after 45 s in multiple planar sections.

4.3 Possible sources of discrepancies

4.3.1 Impact of grid resolution

As mentioned in Section 3.4 the spatial discretisation of the computation domain is one of the most critical points in CFD-modelling. In our case study, the discretisation of the nozzles in the ceiling of the pressure chamber is essential for a good reproduction of the filling process. Searching for reasons for the differences between the physical and the numerical model, the impact of the mesh size for the nozzles was analysed. For that, a grid convergence study was performed for the nozzles. The model used, consists of a section of the pressure chamber and the lock chamber with two rows of nozzles. Different mesh sizes were tested for the grid convergence. For all grids the mesh cells were refined with a series of subsequent bisections. For the nozzle this resulted in an edge length of approximately 0.03 m for coarsest grid, 0.016 m for the medium grid and 0.008 m for the finest grid. For all grids two boundary layer cells were added in the nozzle. As the ratio between the vertical (z-direction, U_z) and the horizontal flow velocity (in x-direction, U_x) in the pressure chamber differs a lot over the complete chamber, five inflow scenarios were tested for each grid. For the comparison the head loss coefficients of the nozzles were evaluated. For the calculation of the head loss coefficients the pressure in the pressure chamber, the pressure above the nozzle and the velocity inside the nozzles were used.
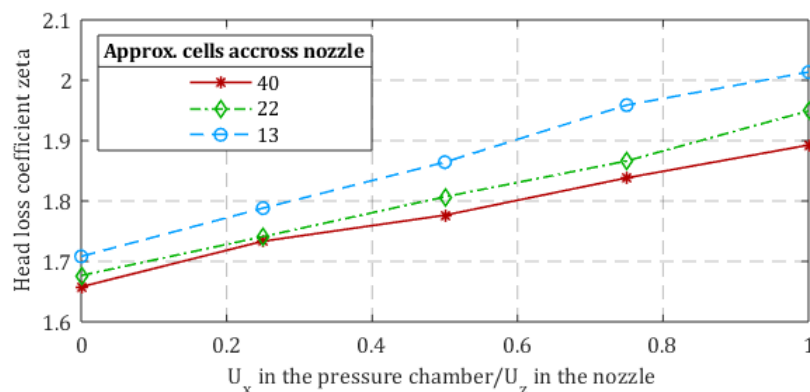

Figure 13: Energy loss of the nozzle with different mesh sizes and different velocity ratios.

The results of the grid study (Figure 13) show that a stronger longitudinal velocity in the pressure chamber increases the head loss, as it is expected. The coarsest grid with only 13 cells across the nozzle shows the biggest head losses for the largest longitudinal velocity in the pressure chamber. The finest grid with 40 cells across the nozzle and the grid with 22 cells across the nozzle provokes comparable head loss results. Especially when the longitudinal velocity is small, the results between the finest and the second finest grid are very similar. Thus, a grid size with 22 cells across the nozzle can therefore be considered as appropriate. However, in the case study the nozzles were only discretized with 13 cells across the nozzle diameter, as this was the only feasible grid resolution concerning time and resources consumption. The analysis of the grid study shows that this might lead to an overestimation of the head losses at the nozzles. This matches with the observed discrepancies in the flowrates as shown in Figure 6.

4.3.2   Uncertainty in the ship position

During the course of the physical model studies it became apparent that the exact transversal position of the ship relative to the lock chamber walls is difficult to measure and to maintain. When the ship is regarded at the low water position in this comparison study, it is ~ 0.8 m (model scale) lower than the upper wall edge of the flume. This makes it difficult for the researcher to measure the distance between ship and wall because a typical arm length is not sufficient to reach this point. Furthermore, due to the quite large vertical lift of the ship, already small errors in the angle of the guiding elevators can lead to a deviated transversal position. And even worse, the walls of the flume tend to bend due to changes of the water loads. Unfortunately, the magnitude of these error sources is not known.

For a further test we assumed that the transversal ship position might have an error margin of ±2 mm (model scale). This equals ±0.05 m in natural scale or ±0.4% of the lock chamber width. We set up two additional numerical models based on the variant with the equivalent sand grain roughness height of 2 mm. In these, we shifted the ship 5 cm to the middle of the lock chamber and 5 cm towards the chamber wall. From Figure 14 we can see that the impact of this small geometric deviation on the transversal forces is rather large. We suspect that the asymmetric position of the ship (Figure 11) causes the jets on the left side of ship to "run around the corner" and result in a pressure drawdown in this area and thus cause the horizontal force. This would explain the reduction of the horizontal force when moving the ship to the middle of the lock chamber.
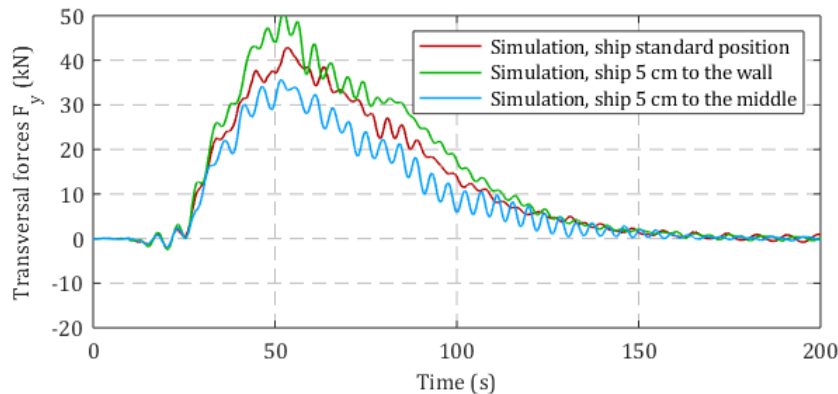

Figure 14: Impact of transversal ship position on transversal forces.

The impact is not as big as the difference between physical and numerical model results but in a comparable range.

4.3.3   Other considerations

The simulations have revealed that a very complex system of jets and vortices is establishing in the pressure chamber. From the numerical model we see that the vortex system in the pressure chamber is dynamic and that the resulting horizontal velocities have an impact on the flow through the nozzles and thus on the ship forces. This seems to be a rather delicate system and thus small changes might have a significant impact.

One source of uncertainty might be the used k-omega-SST turbulence model. Though the model is well established, the complexity of the vortices makes an impact of the turbulence model plausible. Thus, further variants of turbulence

models might be interesting to test. The next step forward would be to test an LES model. But unfortunately, this would require to resolve the major part of the energy transporting eddies with sufficient accuracy on the computational grid. This would require substantial further refinements and thus is not feasible at the time given.

In the physical model, different materials were used to build the filling system. These stayed partially perfectly smooth and in other parts were machined to the desired shape. This results in a varying distribution of roughness which was not prescribed by the construction drawings but originated from the physical model building process. In the numerical model, a constant roughness for all model parts was used. Though the impact of changing the global roughness was small in the numerical model, an uneven distribution might have a bigger impact on the velocity distribution in the jet from the culvert to the pressure chamber and thus on the eddy system.

Another source for possible errors might be hidden in geometry differences between the physical and the numerical models. Though we found one macroscopic geometry glitch in the course of the simulations, it is very well possible that further differences were not found. Furthermore, microscopic glitches might also have an impact on the results. It is very well possible that small edges at the joints of different parts of the physical model have an impact on the flow field and thus on the transversal ship forces.

For the ship in the physical model, the external shape is well defined. In the numerical model, the mass and centre of gravity were setup to match the draught and trim of the ship in the physical model. But the vertical position of the centre of gravity and the moments of inertia of the ship were not known and thus were estimated on the basis of simple formula to be used in the numerical model. These have an impact on the rolling motion of the ship which is typically small in a lock and thus was seen as "not relevant" for deeper considerations in the numerical model. This might be an explanation for the differing oscillation signals for the transversal forces, because the ship might be rolling in the physical model.

A further source of uncertainty is the ship guiding system in the physical model. As described before, the horizontal ship position is difficult to adjust. Furthermore, the elasticity of the guiding system is only partially known. We measured the longitudinal elasticity for one vertical position of the ship and assumed this elasticity to be typical for the system. It can be imagined that this assumption is not correct for the transversal direction or for different vertical positions. This also might be an explanation for the differing oscillation signals for the transversal forces.

5   Lessons learned

For the accuracy of the numerical model the grid generation is crucial: on the one hand the grid resolution plays a major role for the correct modelling of the relevant physical processes, on the other hand it determines the necessary computational effort per time step and additionally limits the time step. Thus, proper grid generation requires substantial effort and sufficient skill of the modeller. The modeller must know a-priori which parts of the model are hydraulically relevant for the system behaviour and thus must focus the necessary efforts on these regions. It is important to have hydraulic understanding in order to judge the quality of the results and thus be able to enhance the numerical model. In the case of this lock simulation study, the grid resolution in the regions of the culvert walls, the pressure chamber and the nozzle inlets are most relevant for a realistic representation of the system's physics. For an appropriate modelling of the wall friction, the space in the culverts has to be discretized with a very fine grid close to the wall. Inside the pressure chamber of the lock a complex system of vortices dominates the flow structure. For a realistic representation of the flow physics within the pressure chamber it is crucial to find a suitable mesh size that allows the modelling of the relevant eddies. Moreover, the hundreds of nozzle inlets also require careful meshing: the grid must be small enough to represent the flow separation at nozzle edges and the head loss, but not too small to avoid too small time steps. This separation at the edge of the inlet has a significant impact on the flow rate of the nozzles. Due to the very small scales this effect is hard to resolve numerically with a sufficient accuracy. It could be a major reason for the observed differences between physical model and numerical model, as this effect occurs mainly on one side (Figure 11) and thus might cause the transversal forces on the ship. For the initialization of the model, the cell surfaces at the water surface of must be as planar as possible in order to avoid initial waves. In our case study we tried to optimize the mesh, so that it fulfils the described requirements. However, as the computational time and resources are limited, the refinements at some parts were still not completely fulfilling our wishes.

From the experience of this and previous case studies with a movable ship within a lock system, it became apparent that a suitable initialization of the simulation is most essential for receiving physically sound results and a stable simulation. As described above (section 3.5) it is necessary to start the simulation with a calm water surface and a balanced ship hull. In the initialization process the centre of mass of the ship hull has to be carefully adjusted, so that the forces cancel each other and the moments on the ship are below an acceptable error margin at the beginning of the simulation. This must be true for at least the timespan of the eigenperiod of the sloshing water in the lock chamber in order to prove that waves from the initialization have no impact on the results.

From the experience of modelling with OpenFOAM® for the last decade we learned that several settings are significantly influencing the accuracy of the results. One important setting is the choice of the numerical schemes for the discretization of the advective terms in the model equations. Generally, second order schemes are recommendable but typically these have rather strict time step limitations. For engineering applications, it can be advantageous to use a blending between second order schemes in areas with small CFL numbers and first order schemes for the small areas of the model with high CFL numbers (see section 3.6).

In our case study, the setup for the fluid structure coupling algorithm had a large impact on the simulation speed, the stability and convergence of the results. Within each step of the iteration cycle for each time step, the movement of the ship must be dampened by a relaxation factor in order to avoid instabilities between the pressure field and the movement of the ship. This relaxation influences the number of iterations that is required in order to achieve a converged solution in each time step. As the number of the outer iterations of the algorithm directly scales the computation time, the modeller wants to keep this number as low as possible. Thus, a careful adjustment of relaxation and iteration numbers is necessary.

From the simulation results we learned, that in the investigated lock system the hydrodynamics of the system can be reproduced much easier than the exact forces on the ship. Particularly the transversal forces are very sensitive to small changes and thus difficult to reproduce. The study showed that several parameters (like e.g. ship position and friction parameters) have a significant impact on the transversal forces, whereas the longitudinal forces could be well reproduced with all tested approaches.

In comparison to the physical scale model, the numerical model allows us to examine the flow structure in detail more easily, as the data of velocity, pressure etc. is available for every point of the simulation domain. Streamlines, vortices and velocity fields can easily be visualized. Yet, the results must be analysed critically and compared to the physical model results. The critical analysis also requires to identify differences between the numerical and the physical model.

Although large effort was put into an accurate construction of the physical model, it is still not an exact representation of the three-dimensional geometry used for the numerical modelling. Differences can result from simple errors, from design simplifications during the building process, from manufacturing precision of the single parts or from the inaccuracies that occur when assembling the model from the pre-manufactured pieces. Additional differences between the physical and the numerical model can result from the inaccurate operation of the valves. Due to the motor drives and the mechanical stiffness of the valve operation system the real valve movement in the physical model does not exactly match the mathematical function which is specified for the operation. The ship force measuring system has mechanical properties which are not perfect and furthermore are not exactly known and thus make reproduction difficult. Data collection and processing can be another source of error in the physical scale model. Here, sensor errors, smoothing or disregarded influences of variable boundary conditions like e.g. temperature dependency can distort the measurement data. Additionally, the processing software for the measured data must be very carefully checked.

We learned that a comparison between a numerical model and a complex physical model, which is more than a "scientific example", is very difficult to perform. It was extremely helpful to have the physical model at hand while the numerical models were setup and run because only that enabled us to check the physical model for its "real" properties. Inexplicable differences between numerical and physical model results required an ad-hoc check of the physical model in order to enhance the similarity between the model setups.

6   Conclusion and future work

In this study, a complex lock filling process with a movable ship was simulated with a 3D-numerical CFD model and the results were compared to physical model results in terms of flow rates, longitudinal and transversal ship forces. Due to the complex geometry the mesh generation process was very sophisticated and required several iterative steps to find a good compromise between a suitable discretization of the relevant flow features and a feasible mesh number and cell size for reasonable computation times. With the fluid structure coupling algorithm of OpenFOAM® the simulations were run in parallel on inhouse high-performance computers. In an iterative manner the necessary settings for the computation were optimized together with further iterations for better meshes.

For the final model, the results showed a very good agreement in terms of flow rates and longitudinal ship forces. In terms of transversal ship forces the results are promising because the system behaviour is reproduced but the accuracy of the peak values is still to be enhanced. A further analysis showed several possible sources for these discrepancies. These might either be on the side of the numerical model (insufficient grid resolution, unsuitable turbulence model), on the side of the physical model (geometric errors, measurement errors, handling errors) or at the exchange between the models (differences in general setup, roughness distribution).

In the future, we plan to further refine the numerical modelling. But we also think that the derived numerical model is good enough to have predictive capabilities. In a first step we want to check how big the influence of the differences between physical model and prototype can be expected to be. Thus, we want to change the model to the prototype viscosity and thus Reynolds numbers and we aim at changing the wall roughness to new and aged concrete. Furthermore, the numerical model has shown that some rather small changes in the setup can have a significant impact on the transversal forces on the ship. In the construction of the prototype we expect small changes compared to the physical model geometry. In order to avoid disadvantageous consequences of these changes, we want to check with the numerical model if changes to the filling system can make the system behaviour more robust against small discrepancies.

Acknowledgements

Author contributions (CRediT)

First author CT: Conceptualization, Formal analysis, Software, Methodology, Investigation, Visualization, Writing-original draft, Writing-review and editing.

Co-first author LS: Data curation, Resources, Software, Supervision, Methodology, Validation, Visualization, Writing-original draft, Writing-review and editing.

Data availability

The geometry files which were the basis for the presented computations are publicly available together with the datasets from the physical model runs used in this study. All data is in prototype scale. It is required to reference this paper, if the data is used in any publication. Data link: https://doi.org/10.48437/02.2021.W.9900.0001

Notation

Name	Symbol	Unit
Face area	A	m^2
Force	F	N
Gravitational acceleration	$\boldsymbol{g}$	m/s^2
Count index	i	-
Resulting moment	$\boldsymbol{M}$	Nm
Surface normal vector	$\boldsymbol{n}$	-
Pressure	p	Pa
Modified pressure	p_{rgh}	Pa
Velocity	$\boldsymbol{U}$	m/s
Velocity transposed	$\boldsymbol{U^T}$	m/s
Artificial compression velocity	$\boldsymbol{U}_c$	m/s
Time	t	s
Height coordinate	z	m
Coordinate vector of a cell or face i	$\boldsymbol{x}_i$	m
Coordinate vector for the centre of rotation of the ship	$\boldsymbol{x}_c$	m
Volume fraction	α	-
Dynamic viscosity	μ	$kg/(ms)$
Density	ρ	kg/m^3

References

Beem, R. C. A., Glerum, A., and Spits, P. L. (2000): Design of locks. Ministerie van Verkeer en Waterstaat, Directoraat-Generaal Rijkswaterstaat, Bouwdienst, Utrecht, Netherlands.

Bleines, W., and Wittmann, H. (1949): Hydromechanische Vorgänge bei der Schleusenfüllung, Deutsche Beiträge. 17. Internationaler Schifffahrtskongreß; Lisbon, Portugal, 1949.

Chevallet, G., Chene, C., Halbardier, A. et al. (2019): Reconstruction and extension of the Mèricourt locks: Study of the hydraulic operation of the structure. In: Smart Rivers 2019 Conference, Lyon, France.

De Jong, R. J. de, and Vrijer, A. (1980): Mathematical and hydraulic model investigation of longitudinal forces on ships in locks with door filling systems. Publication no. 239, Waterloopkundig Laboratorium, Delft, Netherlands.

De Loor, A., Weiler, O., and Kortlever, W. (2013): LOCKFILL: A mathematical model for calculating forces on a ship while levelling through the lock head. In: Proceedings of the PIANC SMART Rivers Conference. 2013.

De Mulder, T. (2009): Mooring forces and ship behaviour in navigation locks. In: PIANC, the World Association for Waterborne Transport Infrastructure (ed.), Innovations in Navigation Lock Design. International Workshop PIANC.

Devolder, B., Schmitt, P., Rauwoens, P. et al. (2015): A review of the implicit motion solver algorithm in OpenFOAM® to simulate a heaving buoy. In: 8th Numerical Towing Tank Symposium (NuTTS'15). 2.-4. Oct 2015, Varna, Bulgaria.

Göbel, G. (2019): Numerical simulation of flow-induced vibration on gates with underflow. 38th IAHR World Congress - "Water: Connecting the World", 1.-6. September 2019. IAHR. Panama City, Panama, 2019, unpublished presentation.

Gonzales, A. O. (2009): Mesh motion alternatives in OpenFOAM: CFD with OpenSource Software. Assignment 3 Göteborg, Sweden.

Jasak, H., Tuković, Ž., Pereira, J. C. F. et al. (2010): Dynamic Mesh Handling in OpenFOAM Applied to Fluid-Structure Interaction Simulations. In: Proceedings of the V European Conference on Computational Fluid Dynamics ECCOMAS CFD 2010, J. C. F. Pereira, A. Sequeira and J. M. C. Pereira (Eds) Lisbon, Portugal,14-17 June 2010.

Kolkman, P. A. (1973): Low-head navigation locks: door filling and emptying systems developed by hydraulic investigations. Publication no. 111. Waterloopkundig Laboratorium, Delft, Netherlands.

Kortlever, W. C. D., van der Hout, A., and Loor, A. de (2015): Hydraulic Studies of the Levelling System for the New Sea Lock at Ijmuiden. In: Bundesanstalt für Wasserbau: Wasserbauwerke - Vom hydraulischen Entwurf bis zum Betrieb, Karlsruhe: Bundesanstalt für Wasserbau, p 31-38.

Krey, H. (1914): Neuere Versuche für Schiffsschleusen. Zentralblatt der Bauverwaltung, 1914.

Menéndez, A. N., Badano, N. D., Lecertúa, E. A., Gerbec, M. S., Re, F., and Re, M. (2010): Computational Fluid Dynamics (CFD) for Hydraulic Design of the Panama Canal Third Set of Locks. In: E. Dvorkin, M. Goldschmit, M. Storti (Eds.), Mecánica Computacional 29(36), pp. 3683-3697. Buenos Aires, Argentina

Menter, F. R., Kuntz, M., and Langtry, R. (2003): Ten Years of Industrial Experience with the SST Turbulence Model. In: K. Hanjalić, Y. Nagano, and M. J. Tummers (eds.), Turbulence, heat and mass transfer 4. Proceedings of the Fourth International Symposium on Turbulence, Heat and Mass Transfer, Antalya, Turkey, 12 - 17 October, 2003 (New York, NY: Begell House).

Nogueira, H. I. S., van der Hout, A., and Kortlever, W. (2019): Hydraulic research for the new lock in Terneuzen. In: Proceedings of the 38th IAHR World Congress - "Water: Connecting the World", 1.-6. September 2019. IAHR. Panama City, Panama, 2019, pp. 4611–4622.

O'Mahoney, T., Heinsbroek, A., de Loor, A. et al. (2018): Numerical simulations of a longitudinal filling system for the New Lock at Terneuzen. 34th PIANC World Congress Panama City, Panama 2018.

Partenscky, H.-W. (1986): Binnenverkehrswasserbau: Schleusenanlagen. Berlin Heidelberg New York Tokyo, Springer.

Pellegrini, F. (2009): Distillating knowledge about SCOTCH. Combinatorial Scientific Computing, Dagstuhl Seminar Proceedings 09061, July 2009.

PIANC (1986): Final Report of the International Commission for the Study of Locks. Edited by PIANC, Brussels, Belgium.

PIANC (2009): InCom WG 29. Innovations in Navigation Lock Design. Edited by PIANC, Brussels, Belgium.

PIANC (2015): InCom WG 155. Ship Behaviour in Locks and Lock Approaches. Edited by PIANC, Brussels, Belgium.

Rodi, W. (2017). Turbulence modeling and simulation in hydraulics: A historical review. Journal of Hydraulic Engineering, 143(5), 03117001.

Roumieu, P., Roux, S., Regge, J. de et al. (2008): Physical Model for the Filling and Emptying System of the Third Set of Panama locks. In: Int. Navigation Seminar PIANC AGA, Brussels, Belgium.

Roux, S., Roumieu, P., De Mulder, T. et al. (2010): Determination of hawser forces using numerical and physical model for the third set of Panama lock studies. In: Proceedings of the 32nd PIANC International Navigation Congress 2010. Liverpool, United Kingdom, 10 - 14 May 2010 (Red Hook, NY: Curran), p 1-15.

Schijf, J. B. (1936): Calcul des forces agissant sur un bateau dans un sas d'écluse, pendant l'éclusage. Bulletin de l'Association Internationale Permanente des Congrès de Navigation, 11/22: 65–100.

Schohl, G. A. (1999): User's Manual for LOCKSIM – Hydraulic simulation of navigation lock filling and emptying systems.

Schulze, L.; Belzner, F.; Hartung, T.; Thorenz, C. (2017): Hydraulische Kriterien für die Dimensionierung von Schleusen. Neue Entwicklungen und künftige Herausforderungen. In Wasserbauliche Herausforderungen an den Binnenschifffahrtsstraßen.

Schulze, L.; Belzner, F. (2021): Aktualisierung der Kriterien für die hydraulische Bemessung von Schleusen. Analyse und Optimierung von Schleusen. Bundesanstalt für Wasserbau. Karlsruhe, Germany (Forschung XPress, 2021_13). Available online at https://izw.baw.de/publikationen/forschung-xpress/0/BAWFoX_2021_13.pdf.

Thorenz, C. (2009): Computational Fluid Dynamics in lock design: State of the art. PIANC International Workshop "Innovation in Navigation Lock Design", 2009 (Brussels, Belgium).

Thorenz, C. (2010): Numerical Evaluation of Filling and Emptying Systems for the New Panama Canal Locks. In: Proceedings of the 32nd PIANC Congress 125th anniversary PIANC – setting the course, Liverpool, UK, 10 - 14 May 2010, pp. 568-589, Brussels, Belgium.

Thorenz, C., and Strybny, J. (2012): On the numerical modelling of filling-emptying system for locks. In: Proceedings of 10th International Conference on Hydroinformatics: HIC 2012: Understanding changing climate and environment and finding solutions, Hamburg, Germany, July 14 - 18, 2012.

Thorenz, C., and Anke, J. (2013): Evaluation of ship forces for a through-the-gate filling system. In: Proceedings of the PIANC-SMART Rivers Conference.

Thorenz, C. (2015): Die NOK-Schleusen als Beispiele für den Einsatz vereinfachter Füllsysteme. In: Bundesanstalt für Wasserbau (Ed.): Wasserbauwerke - Vom hydraulischen Entwurf bis zum Betrieb. Karlsruhe: Bundesanstalt für Wasserbau, pp. 25-30, Karlsruhe, 2015.